Behavioral/Systems/Cognitive

Neural Correlates of High-Gamma Oscillations (60–200 Hz) in Macaque Local Field Potentials and Their Potential Implications in Electrocorticography

Supratim Ray,[1] **Nathan E. Crone,**[2] **Ernst Niebur,**[3] **Piotr J. Franaszczuk,**[2] **and Steven S. Hsiao**[3]

[1]Department of Neurobiology, Harvard Medical School and Howard Hughes Medical Institute, Boston, Massachusetts 02115, [2]Department of Neurology, The Johns Hopkins Hospital, Baltimore, Maryland 21287-7247, and [3]Department of Neuroscience, Zanvyl Krieger Mind/Brain Institute, The Johns Hopkins University, Baltimore, Maryland 21218

Recent studies using electrocorticographic (ECoG) recordings in humans have shown that functional activation of cortex is associated with an increase in power in the high-gamma frequency range (~60–200 Hz). Here we investigate the neural correlates of this high-gamma activity in local field potential (LFP). Single units and LFP were recorded with microelectrodes from the hand region of macaque secondary somatosensory cortex while vibrotactile stimuli of varying intensities were presented to the hand. We found that high-gamma power in the LFP was strongly correlated with the average firing rate recorded by the microelectrodes, both temporally and on a trial-by-trial basis. In comparison, the correlation between firing rate and low-gamma power (40–80 Hz) was much smaller. To explore the potential effects of neuronal firing on ECoG, we developed a model to estimate ECoG power generated by different firing patterns of the underlying cortical population and studied how ECoG power varies with changes in firing rate versus the degree of synchronous firing between neurons in the population. Both an increase in firing rate and neuronal synchrony increased high-gamma power in the simulated ECoG data. However, ECoG high-gamma activity was much more sensitive to increases in neuronal synchrony than firing rate.

Key words: secondary somatosensory cortex; gamma; high-gamma; local field potential; ECoG; synchrony

Introduction

Several EEG and local field potential (LFP) studies have indicated that signal power in the gamma frequency range (30–80 Hz) increases during a variety of cognitive tasks (Fries et al., 2001; Scherberger et al., 2005; Schoffelen et al., 2005; Womelsdorf et al., 2007). Although most studies of gamma oscillations initially emphasized frequencies ~40 Hz, electrocorticographic recordings (ECoG) in patients undergoing epilepsy surgery have suggested that functional activation of cortex is perhaps more consistently associated with a broadband increase in signal power at higher frequencies, typically >60 Hz and extending up to 200 Hz and beyond (Crone et al., 2006). These "high-gamma" responses have been observed in a variety of functional domains, including motor (Crone et al., 1998; Miller et al., 2007), auditory (Crone et al., 2001a; Edwards et al., 2005; Trautner et al., 2006), visual (Lachaux et al., 2005), language (Crone et al., 2001b; Mainy et al., 2007b), and attention (Tallon-Baudry et al., 2005; Jung et al.,

2008; Ray et al., 2008a). However, the relationship between these high-frequency gamma oscillations and the firing properties of the neural population remains unclear. Here we investigate this relationship in the LFP that measures the activity of a small population of neurons near the microelectrode, and in a model of ECoG that simulates the average activity of a much larger number (~500,000) of neurons.

In a previous study (Ray et al., 2008b), we measured the correlation between spikes and oscillations in the LFP recorded in secondary somatosensory cortex (SII) of awake macaque monkeys, and we found that spikes were tightly correlated with oscillations in the high-gamma range. Based on those results, we hypothesize here that LFP high-gamma activity represents the average firing of neurons near the microelectrode from which the LFP activity is recorded, weighted according to their distance from the electrode. We test this hypothesis by studying the covariations of population firing and LFP high-gamma over time, as well as trial-by-trial covariations in these two quantities. We show that the two quantities are tightly correlated.

If LFP high-gamma activity is a measure of neural firing of the population near the microelectrode, ECoG high-gamma activity should be an indicator of the firing properties of the entire neural population under the ECoG electrode. However, for such a large network of neurons, the temporal pattern of firing (in particular, neural synchronization) may be important. We develop a model to estimate ECoG high-gamma power under different firing rate profiles of the neural population and compare the increase in

high-gamma activity attributable to an increase in population firing rate versus an increase in synchronization. Although both increases in firing rate and synchrony lead to an increase in high-gamma power in the simulated data, the effect of a 10-fold increase in firing rate is matched by that of a small (~1%) increase in synchrony. Thus, ECoG high-gamma activity is likely more sensitive to synchronous firing in the underlying cortical neural population than to the underlying firing rate.

Materials and Methods

The experimental design, recording setup and some of the analysis methods are described in detail in the study by Ray et al. (2008b). Here, we describe them briefly.

Animals and animal behavior. Single-unit recordings were obtained from secondary somatosensory cortex in two macaque monkeys (*Macaca mulatta,* one female, 4–6 kg). The monkeys were water restricted and received most of their daily water during the experiment. They were trained to sit quietly in a primate chair during the experiment with their hands supinated and restrained. Water rewards were given at pseudorandom intervals during the experiment to keep the animals awake and alert. All procedures and experimental protocols complied with the guidelines of the Johns Hopkins University Animal Care and Use Committee and the National Institutes of Health *Guide for the Care and Use of Laboratory Animals.*

Experimental design. Tactile stimuli were delivered perpendicular to the skin through a probe on the distal pad of the second or third digits (D2 or D3) by a vibratory stimulator (Mini-shaker, model 4810; Brüel & Kjær). The Mini-shaker stimulator produced a sinusoidal vibration, which was presented for 1 s, with an interstimulus interval of 1.2 s. Three different stimulus frequencies (50, 100, and 200 Hz) and four different amplitudes (in the ratio 1:2:5:10 and denoted by G1, G2, G5, and G10 throughout this study) were used, with 50 trials per frequency and amplitude combination. Stimuli were presented in a pseudorandom order. Stimulus amplitude at the lowest amplitude (G1) was approximately five times higher than the perceptual threshold (on average ~5, 3, and 0.8 μm at 50, 100 and 200 Hz, respectively). Mini-shaker movements were monitored using an accelerometer (Type 8636C5; Kistler Instrument) and the corresponding displacement amplitudes were computed by double integration of the acceleration. In this study, only the results for stimulus frequency of 50 Hz are shown because SA1 (slowly adapting) and RA (rapidly adapting) receptors found in the periphery respond more strongly to stimulus frequencies at or below ~50 Hz. Similar results were obtained at other stimulus frequencies.

Recordings. Stainless steel recording cylinders were placed surgically on each hemisphere over SII using aseptic procedures under sodium pentobarbital anesthesia (25 mg/kg, i.v., initial dose plus 5–15 mg/kg/hr, i.v.). Neural recordings were started not earlier than 1 week after surgery, to allow sufficient time for recovery. Neural activity was recorded using seven platinum-iridium extracellular microelectrodes spaced 400 μm apart and driven by a Reitboeck microdrive (Mountcastle et al., 1991). The signals from the seven channels were amplified by a headstage amplifier (10×) and divided into two streams for the collection of LFP and spikes, respectively. One of the streams was amplified (100×) and filtered (0.3–300 Hz, 6 dB/octave) using Grass amplifiers (Model 15 LT with 12A54 Quad amplifiers; Grass-Telefactor/Astro-Med). The second input stream was bandpass filtered (500–1000 Hz), amplified (10× to 100×), and spikes were isolated using a window amplitude discriminator. Only neurons whose action potentials were well isolated from noise were selected for analysis. As a control, to ensure that the observed activity was not an artifact, we repeated the experiment for several neurons after taking the stimulator off the finger. For such trials, all stimulus-related activity disappeared.

Two hundred and three neurons were recorded from three hemispheres (55 and 71 neurons from hemispheres 1 and 2, respectively, of monkey 1; and 77 neurons from one hemisphere in monkey 2).

Time-frequency analysis. Time-frequency analysis was performed using the matching pursuit (MP) algorithm (Mallat and Zhang, 1993). MP is an iterative procedure to decompose a signal as a linear combination of members of a specified family of functions $g_{\gamma n}$, which are usually chosen to be sine-modulated Gaussians, i.e., Gabor functions or "Gabor atoms," because they give the best compromise between frequency and time resolution. In this algorithm, a large overcomplete dictionary of Gabor atoms is first created. In the first iteration the atom $g_{\gamma 0}$ which best describes the signal $f(t)$ (i.e., has the largest inner product with it) is chosen from the dictionary and its projection onto the signal is subtracted from it. The procedure is repeated iteratively with the residual replacing the signal. Thus, during each of the subsequent iterations, the waveform $g_{\gamma n}$ is matched to the signal residue $R^n f$, which is the residue left after subtracting the results of previous iterations. Mathematical details of this method are presented in Ray et al., 2008b. Time-frequency plots were obtained by calculating the Wigner distribution of individual atoms and taking the weighted sum (Mallat and Zhang, 1993). We have made the software used for MP computation online at http://erl.neuro.jhmi.edu/mpsoft.

The LFP was originally sampled at 5 kHz and then down-sampled to 1 kHz. Matching pursuit was performed on signals of 2048 bins (−0.523–1.524 s at 1 ms resolution, where zero denotes the time of stimulus onset), yielding a 2048 × 2048 array of time-frequency values (with a time resolution of 1 ms and frequency resolution of 500/2048 Hz). This was further down-sampled by a factor of 8 (the mean of every 8 × 8 pixels was taken as one time-frequency bin), yielding a time resolution of 8 ms and a frequency resolution of ~2 Hz. For the study of temporal variations in power, no down-sampling was performed so that time resolution was 1 ms.

Noise and stimulus artifact removal. With MP, line noise (60 Hz and harmonics) are represented by long atoms (spread parallel to the time axis) concentrated ~60 Hz and its harmonics. Similarly, a sinusoidal stimulus artifact is represented by long atoms concentrated at the stimulus frequency and harmonics. Such atoms were excluded from the analysis to eliminate these artifacts. This procedure is more powerful than traditional filtering because at least some of the energy at 60 Hz that has a physiological origin is preserved. For example, a short burst of activity, which MP represents as an atom localized in time but spread in frequency, will not be excluded from analysis.

For each neuron, noisy trials were eliminated before analysis by visual inspection and window discrimination of the filtered LFP. For each stimulus frequency and amplitude combination, between 25 and 50 trials were analyzed (on average, ~3 trials of 50 were eliminated).

Selection and classification of neurons. We tested whether the firing rates and signal power were stable over time to ensure that the results were not biased by a change in the level of alertness/attention of the monkey over the recording period. Using regression analysis, we selected 141 neurons for which firing rates and gamma power were stable for the entire recording duration (Ray et al., 2008b). These neurons were categorized into three categories based on their firing rate profiles: Excited (for which the firing rate increased after stimulus onset; 78 neurons), Inhibited (firing rate decreased after stimulus onset; 21 neurons), and Not-Driven (no change in firing rate; 42 neurons). In this report we use the Excited population to study temporal and trial-by-trial correlations between population firing rate and signal power in different frequency bands.

Frequency bands. The term "gamma band" is used here to describe the broad frequency range between 40 and 200 Hz. We analyzed the frequency band between 60 and 150 Hz (called the "high-gamma" band) because the spike-triggered average had prominent power in this range (Ray et al., 2008b). Additionally, we also performed the analysis on the traditional "low-gamma" frequency band between 40 and 80 Hz, and in the beta frequency range (16–24 Hz) where we observed a consistent decrease in power after stimulus onset. For low and high-gamma power, several different frequency ranges were used (80–150 Hz and 60–200 Hz for high-gamma, 40–60 Hz for low-gamma) and very similar results were obtained.

Cross-correlation analysis. We adopted the method used by Womelsdorf et al. (2007) based on Spearman-rank correlation to compute the cross-correlation between mean normalized firing rates and mean normalized power in different frequency bands. As a measure of the cross-correlation at time lag L, we computed the Spearman-rank correlation between the power between 0 and 200 ms and the firing rates from L to L + 200 ms (both quantities were computed with a time resolution of 1 ms,

thus we obtained 200 data pairs). This method is approximate because the power and rate values are not independent across time. However, the Spearman rank correlation analysis avoids assumptions about the underlying distributions (Womelsdorf et al., 2007). We obtained cross-correlation functions for time lags L between -100 and 100 ms. Because the time lag of the rate changes was defined relative to the power changes, a peak at negative time lag indicates that firing rate changes precede power changes.

ECoG data modeling. We estimated the change in high-gamma power in the ECoG signal that is due to changes in firing rate or synchronization in the underlying neural population. Most of the power recorded by the ECoG electrode is due to synaptic activity (Nunez, 1981, 1995), so the contribution of the action potentials is small and limited to the higher frequencies only. However, here we were specifically interested in the contribution of action potentials and their time-locked LFP components, and thus limited the analysis to the effect of neuronal firing on the ECoG activity.

Suppose a microelectrode records the activity of a neuron as shown in supplemental Figure 1, available at www.jneurosci.org as supplemental material. This neuron is at a distance R from the dura (and hence from the ECoG electrode). When the neuron fires an action potential, the microelectrode records the extracellular action potential waveform $\psi(t)$ (which is estimated by the spike-triggered average), whereas the ECoG electrode records the potential $\Phi(t)$. The problem is to find a relationship between $\Phi(t)$ and $\psi(t)$. Because a complete characterization of $\Phi(t)$ with respect to $\psi(t)$ is extremely difficult, we make a series of approximations to model a relationship between the two. The overall potential due to all the underlying neurons is then computed using linear superposition. The approximations are explained below.

Passive recording system. The presence of the ECoG electrode influences the electric field generated by the neuronal population. Because the conductance of the electrode is extremely high (ECoG electrodes are typically made of platinum-iridium) compared with the brain tissue, it constrains the entire cortical surface (on which it is placed) to have the same potential. To compute this potential, first the induced charge on the metal electrode must be computed (the induced charge will develop to keep the potential the same over the entire area of the electrode). In general, the solution depends on a number of factors, including the position of the current source (neuron) with respect to the electrode, the dimensions of the electrode, the geometry of the neuron, as well as the input impedance of the recording system. This problem is extremely difficult to solve for the entire neural population. Thus, we approximate the potential of the ECoG electrode by a point recording contact situated directly above the current source (for example, for the neuron shown in supplemental Fig. 1, available at www.jneurosci.org as supplemental material, we assume that the recording contact is at a distance R from the soma and situated vertically above the neuron).

Current source localization. To compute the potential recorded at any distance from the neuron, first the distribution of the currents must be computed. These current sources and sinks are generated because of the synaptic activity (for example, opening of sodium channels will create a local current sink). Once an action potential is generated, it propagates along the axon as well as the dendrites, creating a distribution of local sources and sinks. However, detailed numerical calculations have shown that the currents at/near the soma are typically much larger than the currents in the dendrites, whereas the contribution of the myelinated part of the axon to the extracellular potential is negligible (Gold et al., 2006). Furthermore, the potential decays quickly below the level of detection as the microelectrode moves away from the soma (Gold et al., 2006). Thus, the main contributions to the recorded potentials are due to currents generated close to the soma, and we therefore assume that in all the microelectrode recordings, the electrode is situated close to the soma. Gold (2006) further showed that for microelectrodes close to the soma, the temporal profile of the potential and of the current sources is very similar. This is expected, because given a point source I in an unbounded and isotropic volume conductor, the corresponding potential at a distance r is given by

$$\psi = \frac{\rho I}{4\pi r} \tag{1}$$

where ρ is the extracellular resistivity. Thus, $I(t)$ is proportional to $\psi(t)$ (both have the same shape).

Current source distribution. If the potential recorded by a microelectrode is considered to be due to a point current source at the soma, the potential will decrease as $1/r$ from the current source (Eq. 1). However, once the action potential is initiated at the axon initial segment, the charge imbalance depolarizes the nearby membrane (which allows the action potential to propagate). The fall-off of the potential with distance is critically dependent on the spatial distribution of these local current sources and sinks. For example, the spatial distribution of currents can be approximated by a current sink flanked on each side by a current source, i.e., a triphasic current source distribution (Malmivuo and Plonsey, 1995). In general, the resulting potential has a multipole expansion with a leading $1/r^2$ term (and if the triphasic current source is perfectly symmetric, a leading $1/r^3$ term). Omitting higher terms of the multipole expansion, we approximate the effect of the spatial distribution of currents on the potential by using the following equation:

$$\psi(t) = \frac{\rho I(t)}{4\pi r^n} \tag{2}$$

where n is an exponent between 1 and 3. Here, $n = 1$ represents a point source (no redistribution of charge), $n = 2$ a dipole (two equal and opposite current sources), and $n = 3$ represents the quadrupole moment, e.g., resulting from an instantaneous symmetric distribution of charge into a point sink of $I/2$ flanked by two point sources of $-I/4$. The simulations are performed for different values of n. Equation 2 is another approximation because in general the extracellular potential $\psi(t)$ and the current source $I(t)$ may be related in a complicated way that may depend on a variety of factors, like redistribution of charge along the membrane (the trans-membrane current), the contribution of the current sources in the dendrites and so on. It must be noted that regardless of the rate of decay of the potential with distance, the shape of the extracellular action potential is preserved, because at lower frequencies (at least up to the high-gamma range) the brain acts like a purely resistive medium and the conductivity is not frequency dependent (Nunez, 1981; Logothetis et al., 2007). Therefore, we relate the ECoG potential $\Phi(t)$ with the extracellular action potential $\psi(t)$ using the following equation:

$$\phi(t) = C\frac{\psi(t)}{R^n} \tag{3}$$

where R is the distance between the ECoG electrode and the soma. The constant C incorporates several factors like the distance between the soma and the microelectrode, the conductivity of the medium, size of the soma, and the orientation of the current sources, whereas the exponent n incorporates, approximately, the spatial distribution of the charge along the membrane near the axon initial segment. From linear superposition, the overall ECoG potential due to a population of N neurons (with the soma of the kth neuron located at a distance R_k from the ECoG electrode) is given by

$$\phi(t) = \sum_{k=1}^{N} C_k \frac{\psi_k(t)}{R_k^n} \tag{4}$$

Spatial distribution of neurons. The somatosensory cortex has an overall thickness of ~ 2 mm (Noctor et al., 2001). The contribution of cortical neurons to the ECoG potential depends on a variety of factors such as their type, density, orientation, size and pattern of interconnections. Layer 1 (the molecular layer) mainly contains the apical dendritic extensions of the cells in layers 2/3 or axonic connections from other columns and only a few neuronal cell bodies. Pyramidal cells are found in Layers 2/3 as well as Layer 5, whereas Layer 4 has prominent spiny stellate neurons that receive input from thalamic neurons. It is unclear how the size or the type of a neuron affects the potential observed at the ECoG electrode. Gold et al. (2006) showed that the potential depends on the
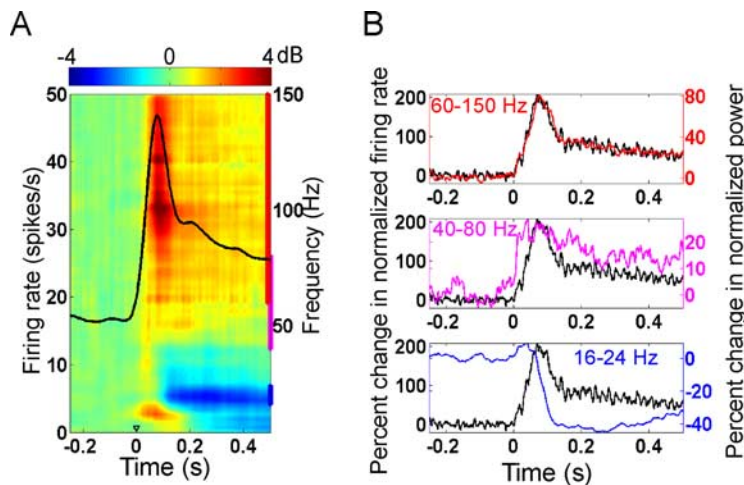
Figure 1. Temporal dynamics of firing rates and LFP oscillations. **A**, Time-frequency plot of the change of the LFP power relative to baseline (in dB), plotted along with the firing rate of the Excited population at the highest stimulus intensity (overlaid black curve). Time $t = 0$ indicates stimulus onset. The blue, magenta, and red vertical bars on the right edge of the plot indicate the frequency ranges for beta, low-gamma, and high-gamma power, respectively. **B**, Change in normalized firing rates (black traces) plotted along with the change in normalized power in the high-gamma (red, top), low-gamma (magenta, middle), and beta (blue, bottom) frequency ranges.

size, but not on the type of neuron or the extent of dendritic arborization. However, an important criterion seems to be the conductance of ion channels. As an approximation, we ignore the laminar differences and assume that the neurons beneath the ECoG electrodes form a homogeneous population. Most commonly used ECoG electrodes have a diameter of 4 mm with an exposed surface of diameter 2.3 mm. The density of neurons in human cortex is $\sim 10^5/mm^2$; the ECoG electrode with an exposed area of 2.3 mm diameter will thus have $\sim 500,000$ neurons under it. We assume that these neurons are situated at depths between 0.2 and 2 mm (i.e., they are uniformly distributed between Layers 2 through 6). The diversity in cell size/type/conductivity/orientation is incorporated by varying the coefficient C in equation 4 randomly between 0 and 1 (uniformly distributed).

In summary, we make the following assumptions to estimate the ECoG potential ($\Phi(t)$) from the microelectrode action potentials ($\psi(t)$), obtained by taking the mean spike-triggered average of the excited population in the early stimulus period):

The ECoG electrode does not influence the electric field generated by the neurons.

The microelectrode is close enough to the soma such that only the currents in the soma influence the potential $\psi(t)$. This makes the current source proportional to the potential (Eq. 1).

The effect of current distribution in the dendrites and axon is modeled by assuming that the potential drops off as $1/r^n$, where n is between 1 and 3. The value of n is critically dependent on the spatial distribution of charge, $n = 1$ corresponds to no distribution of charge (just a point current source at the soma), whereas $n = 3$ corresponds to a perfect instantaneous redistribution into a sink of size $I/2$ flanked by two symmetric sources of size $I/4$. Higher terms in the multipole expansion are ignored.

The laminar differences are ignored, and the differences in cell size, type, orientation, conductivity and density are incorporated using a single variable (C; Eq. 4) that is uniformly distributed between 0 and 1.

In supplemental Discussion 2, available at www.jneurosci.org as supplemental material, we address some of these assumptions in detail and discuss experimental and computation strategies to improve the model.

Results

Temporal dynamics of firing rate and LFP power

To test the hypothesis that LFP high-gamma power is tightly coupled with the average firing rate of the neural population near the microelectrode, we compared the temporal dynamics of the mean time-frequency power changes with respect to a baseline period (-200 to -50 ms, where 0 indicates stimulus onset) in the LFP of the "Excited" population (see Material and Methods for details) with the mean firing rates of this population. Figure 1A shows the time-frequency energy difference plot for the Excited population at a stimulus amplitude of G10, as well as the firing rate of the Excited population. Both low- and high-gamma power increased with an increase in firing rate. To quantify these results, we first normalized the firing rate of each neuron by dividing it by the maximum firing rate for that neuron. These normalized firing rates were then averaged across the Excited population to obtain the mean normalized firing rates. Similarly, we computed the mean normalized power in the following three different frequency bands: beta (16–24), low-gamma (40–80 Hz), and high-gamma (60–150 Hz). Figure 1B shows the percentage of change in normalized firing rates from baseline firing rates as well as the percentage of change in normalized LFP power from baseline power, for the high-gamma (top), low-gamma (middle), and beta (bottom) frequency bands. We observed a strong correlation between the high-gamma power and firing rates curves, suggesting a close and possibly causal relationship. Low-gamma power also increased after stimulus onset, but the increase was smaller (scale in Fig. 1B is different for different frequency bands) and stayed constant for a longer duration. The decrease in beta power started at the same time as, or slightly after, the firing rate started to increase. The results were similar when the analysis was repeated without normalization of firing rates or power.

To test whether the changes in firing rate preceded the changes in power in Figure 1B, we computed the cross-correlation between mean normalized firing rates and mean normalized LFP power (see Materials and Methods). Figure 2 shows the cross-correlations between the normalized firing rates and normalized high-gamma (left), low-gamma (middle) and beta (right) power, for the four stimulus amplitudes. The time periods at which the cross-correlation was significant (Spearman rank test, $p < 0.05$, Bonferroni corrected for multiple comparisons) are denoted by horizontal lines at the bottom of each plot. We observed a strong correlation of firing rates with high-gamma power, with a correlation coefficient of 0.92 at the highest stimulus amplitude (G10). Except for the smallest stimulus amplitude (for which the cross-correlation was much smaller), the peak of the cross-correlation between firing rates and high-gamma power occurred at negative latencies (-6, -3, and -4 ms for G2, G5, and G10, respectively). This indicated that changes in firing rates preceded changes in power, and the time lags were consistent with the lags reported previously [Ray et al. (2008b), their Fig. 6C]. The cross-correlation values between firing rates and low-gamma power were much smaller (Fig. 2, middle). The peak occurred at a positive time lag (~ 18 ms for G10), showing that low-gamma power increases before the increase in firing rate.

We also observed a strong correlation between firing rates and beta power. As shown in Figure 1B, bottom, beta power begins to decrease ~ 40 ms before the firing rate reaches its maximum value, and correspondingly the cross-correlation shows a peak at

~40 ms at G10 (black trace). The lowest level of beta power, however, is reached after the firing rate peaks.

Trial-by-trial analysis

If the firing rates and LFP power in a frequency band are related to each other, they should covary on a trial-by-trial basis. To test this hypothesis, we computed the Spearman rank coefficient between the firing rates and LFP power recorded from individual sites. However, although the LFP represents the contribution of several neurons near the microelectrode, the firing rate is recorded for an individual neuron (often the one closest to the microelectrode so that the action potential can be easily isolated). As a result, these correlations are expected to be smaller than the temporal correlations that were computed between the average firing rates and LFP power of the Excited population.

The analysis was performed on 72 Excited neurons from which we had recorded at least 40 trials for each stimulus amplitude condition. The mean firing rates and power in the "early stimulus period," defined in the interval 50–200 ms post stimulus, were used because the firing rates were much higher in this period and there was more variability across trials. Figure 3 shows the histogram of the Spearman rank correlation between the firing rates and high-gamma (left), low-gamma (middle), and beta (right) power, computed for each neuron (i.e., the correlation was computed for 40 data points for each stimulus amplitude). We found a positive correlation between high-gamma power and firing rates, so that the histograms shown in the left panel of Figure 3 were shifted toward the right side of the origin. The neurons for which the correlation coefficient was significant ($p < 0.05$) are shown in black (31, 28, 26, and 26 neurons of the 72 studied were significant for stimulus intensity of G1, G2, G5, and G10 when no Bonferroni correction was applied. Because the variability across trials was high at individual sites, only 4, 6, 3, and 5 neurons were significant after Bonferroni correction for G1, G2, G5, and G10, respectively). For low-gamma or beta, the correlation coefficients were much smaller. Only 12, 12, 8, and 9 (0, 3, 0, 1 after Bonferroni correction) neurons had significant correlations for the low-gamma (middle), and only 8, 7, 6, 5 (none after Bonferroni correction) neurons were significant for beta power (right). Because the beta suppression began only after ~200 ms, we recomputed the correlation after taking the average power between 250 and 500 ms. Similar results were found (9, 5, 2, and 2 neurons were significant for G1, G2, G5 and G10, respectively; only 1 neuron at G2 was significant after Bonferroni correction).

Although these correlations were small when computed for individual neurons (40 data points per stimulus amplitude), the results were highly statistically significant when the correlations were computed for the entire dataset of all neurons and all trials (i.e., when computed over 40 × 72 = 2880 data points). To account for the variability between neurons recorded from different sessions, the firing rates and power for each neuron were normalized by dividing by the maximum firing rate/power for the entire set of trials for any of the four stimulus amplitudes. After normalization, for each neuron we obtained 160 data points (40 data points for each stimulus amplitude), with a maximum
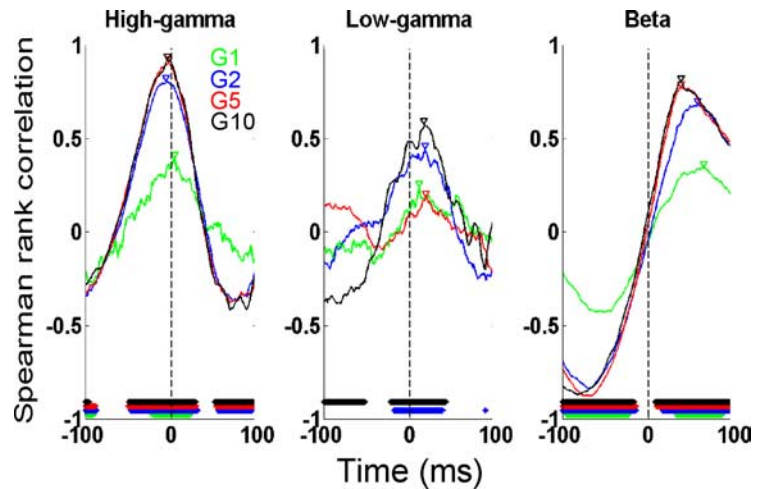

Figure 2. Cross-correlation analysis between the normalized firing rates and normalized high-gamma (left), low-gamma (middle), and beta (right) power, for the four stimulus amplitudes (indicated by different colors). The time periods at which the cross-correlation is significant (Spearman rank test, $p < 0.05$, Bonferroni-corrected for multiple comparisons) are denoted by horizontal lines at the bottom of each plot. Negative latencies indicate that changes in firing rates preceded changes in power. Triangles indicate the time when the cross-correlation is highest.

value of unity. These data points were then analyzed separately for each of the four stimulus amplitudes (72 × 40 = 2880 data points for each amplitude) (supplemental Fig. 2, available at www.jneurosci.org as supplemental material). We then performed a regression analysis to test for a possible relationship between normalized firing rates and normalized power. The p values of the slope between rate versus high-gamma were highly significant (slopes: 0.23, 0.22, 0.14, and 0.17; p values $<10^{-41}$, 10^{-43}, 10^{-21}, and 10^{-28} for G1, G2, G5 and G10, respectively). Even for low-gamma, the p values were highly significant (slopes: 0.16, 0.12, 0.10, and 0.10; p values: 10^{-17}, 4.2×10^{-14}, 2.1×10^{-11} and 8.5×10^{-13}). For rate versus beta power, the slopes were 0.02, 0.02, 0.06 and 0.05, and p values were 0.34, 0.25, 9.6×10^{-6} and 3.4×10^{-4} when the power was computed between 50 and 200 ms post stimulus. We were concerned that the significant correlations at G5 and G10 were artifacts of the phase-locked activity (Fig. 1A, the red-orange spot at low frequency), and we computed the power also between 250 and 500 ms, when beta power suppression was more evident. In this case, the slopes were 0.006, 0.003, 0.002, and 0.023, and p values were 0.77, 0.86, 0.85, and 0.03.

The results obtained from trial-by-trial variability analysis, although computed under some approximations, are consistent with the results obtained from the temporal correlation analysis that showed that high-gamma power is much more tightly correlated with the firing properties of the neural population than low-gamma or beta power. These results are consistent with our previous finding that each action potential is tightly coupled to LFP activity in the high-gamma range (Ray et al., 2008b), because in that case an increase in firing rate would lead to a corresponding increase in high-gamma power generated by the neural population near the microelectrode.

Next, we studied the neural correlates of high-gamma activity when recorded at a higher level of integration, as in ECoG recordings in humans, which typically record from ~500,000 neurons. For such recordings, the temporal structure of firing in the population may be important. As mentioned earlier, both an increase in the firing rate and an increase in synchrony in a population of neurons could theoretically lead to an increase in high-gamma activity. To compare the effects of these two aspects of neural
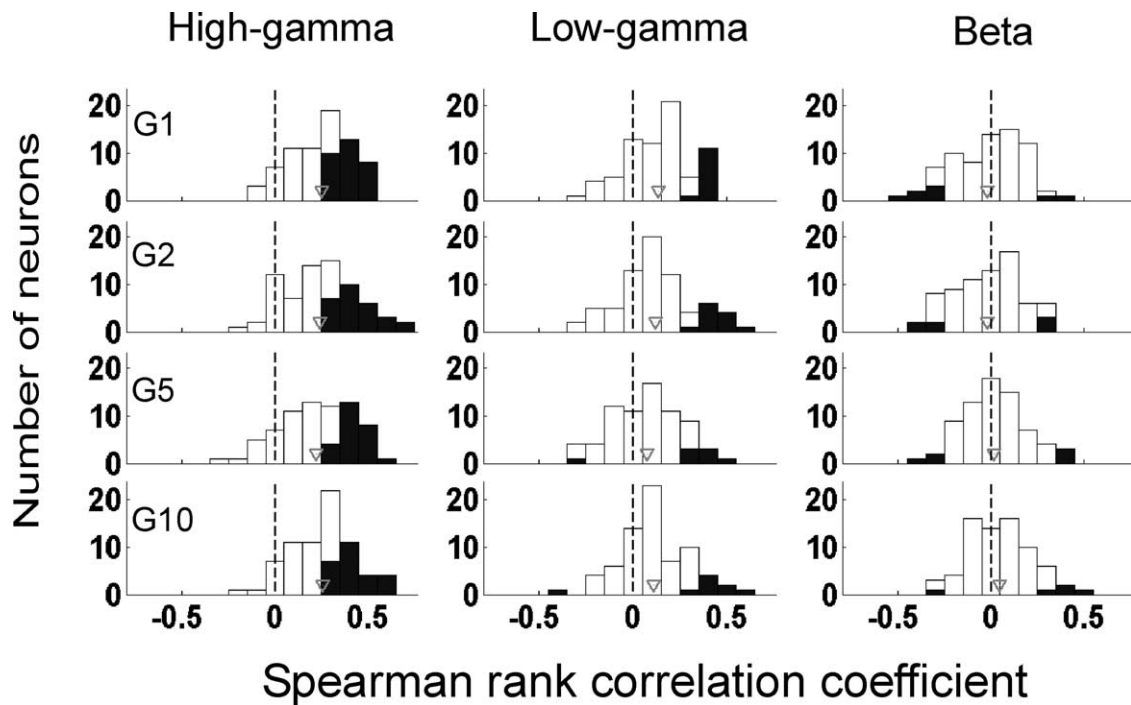
Figure 3. Histograms of Spearman rank correlation values between firing rates and LFP power for individual neurons in the Excited population. Power was computed for three frequency bands (as in Fig. 1) and four stimulus intensities (as in Fig. 2). Neurons for which the correlation was significant ($p < 0.05$, Spearman rank test) are shown in black. Gray triangle indicates the mean correlation for the entire Excited population.

activity on ECoG high-gamma power, we developed a model to estimate ECoG potential under different assumptions about the firing patterns of the underlying neural population (see Materials and Methods). The results are described in the next section.

Modeling of ECoG data

Figure 4A shows the results for a population of $N = 10^5$ model neurons that fired randomly with a constant firing rate (following a Poisson distribution), which was varied between 10 and 100 spikes/s (top row). The model exponent (n in Eq. 2) was set to 2. The corresponding simulated ECoG signals are shown in the middle row, and the time-frequency spectra of the ECoG (average of 50 simulated trials) are shown in the bottom row. Figure 4B shows the same results for a population of 10^5 neurons in which a subpopulation of neurons fired synchronously while the firing rate remained constant at 10 spikes/s. The percentage of neurons that fired synchronously was increased from 0 to 5% (from left to right). A comparison of the high-gamma power under these two conditions (Fig. 4C) showed that the increase in ECoG high-gamma power that was obtained from a large increase in firing rate could be obtained by a small increase in synchronization. For example, an increase in high-gamma power due to a 10-fold increase in firing rate is the same as that caused by a 2% increase in synchronization. Figure 4D shows the percentage of synchronously firing neurons that was required to explain a 10-fold increase in firing rate in the asynchronous population, as a function of the neural population and the model exponent (Eq. 2). For a population of 5×10^5 neurons, <1% synchronization was required to achieve the same increase in high-gamma as generated by a 10-fold increase in firing rate, for all tested values of the model exponent. These results are in agreement with theoretical arguments suggesting that the ratio of activity of a coherent subpopulation of size M and an incoherent subpopulation of size L is $M/\sqrt{L}$ (Nunez, 1981, 1995) (the ratio of power,

approximated by the square of the amplitude, is thus M^2/L). In Appendix 1, we use a simple argument based on the variance in firing rate to show that for a neural population of size N, the ECoG power for the asynchronous condition is proportional to N, whereas for the synchronous condition it is proportional to N^2.

Figure 4B shows the effect of a particular type of synchronization, where a fraction of neurons fired with perfect synchrony although the remaining population was asynchronous. Next, we considered a population of neurons in which any two spike trains have a correlation coefficient of χ (such spike trains can be generated using a technique described by Mikula and Niebur, 2003). Figure 5A shows the increase in high-gamma power as the correlation coefficient is increased from 0 to 0.00045, whereas Figure 5B shows the correlation coefficient required to achieve the same increase in high-gamma as generated by a 10-fold increase in firing rate under different model parameters. Figure 5, A and B, are thus analogous to Figure 4, C and D, with the percentage synchronization replaced by the correlation coefficient. Thus, an increase in high-gamma due to a 10-fold increase in firing rate in a population of independently firing neurons is equivalent to an increase in the pairwise correlation coefficient from zero (independent firing) to <0.0004. Experimental measurement of this level of synchrony in a population would be difficult using single-unit pairwise cross-correlation measures because the correlation values would be very small. High-gamma activity could be a better and more robust marker of synchronization in large networks of neurons. This is further elaborated in Discussion.

To directly compare the effects of rate and synchrony on ECoG high-gamma power, an experimental paradigm would have to be designed in which firing rate and synchrony/correlation could be varied independently of each other. However, these quantities are usually correlated with each other (de la Rocha et al., 2007). Studies of selective attention provide a partial solution, because in such studies a substantial increase in pairwise syn-
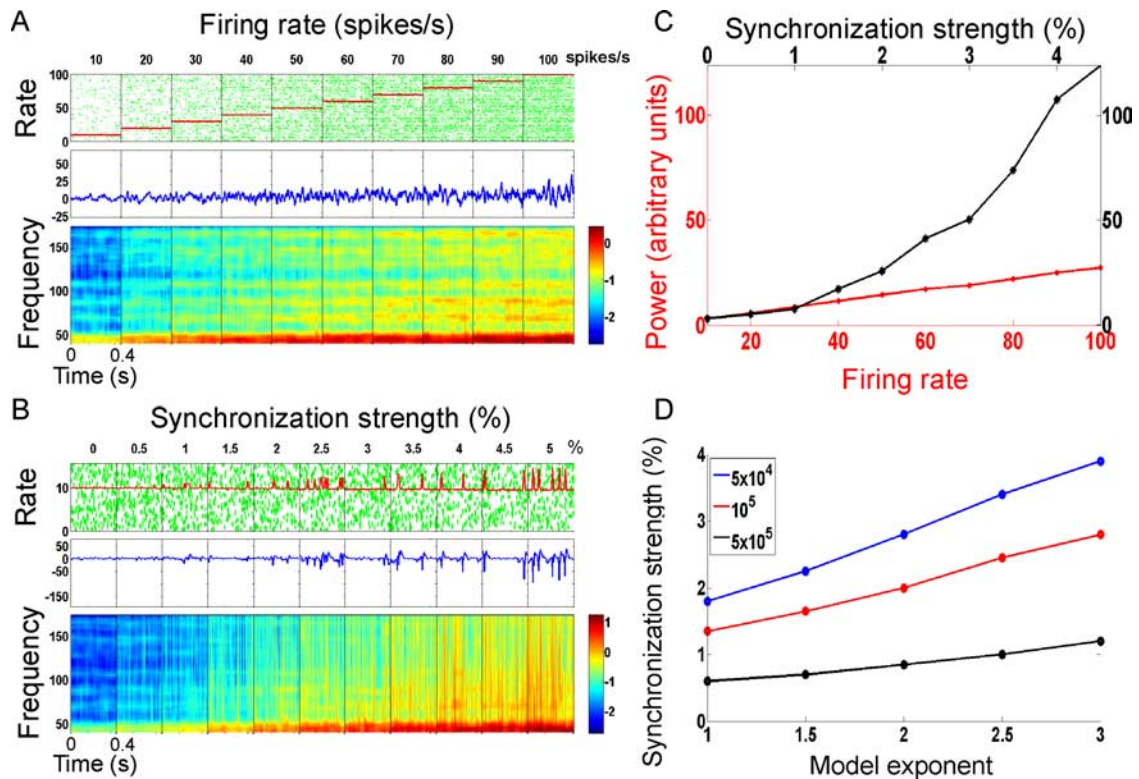
Figure 4. ECoG modeling results. For plots *A–C*, the total number of neurons is 10^5 and the model exponent (*n* in Eq. 2) is 2. *A*, Top row shows example raster plots of simulated spike trains with random firing (a representative set of 50 spike trains is shown). The 10 panels correspond to 10 different simulations for which the firing rate was fixed between 10 and 100 spikes/s. The numbers on top of the panel indicate the theoretical firing rate in spikes/s. The instantaneous firing rate (computed from the rasters) is shown in red. The middle row shows the simulated ECoG signal for each simulation. The bottom row shows the time-frequency power spectrum (in dB) of the ECoG (50 simulations like the one shown in the top were averaged, consistent with the number of trials averaged in LFP data and a previous ECoG study). *B*, Same panel configuration as in *A*; the simulated spike trains all have a mean fixed firing rate of 10 spikes/s, but a subpopulation of the neurons fire in synchrony. The percentage of synchronously firing neurons increase from 0 to 5% from left to right (indicated by the numbers on top of the panel). *C*, High-gamma power (60 –150 Hz) for the simulations with increasing firing rate (red) and increasing synchronization (black). *D*, The synchronization strength required to match the high-gamma power of a randomly firing population with a firing rate of 100 spikes/s, for different values of *N* (size of the neural population; colored lines as labeled in legend) as a function of the model exponent.

chrony has been reported with only a modest increase in firing rate (Steinmetz et al., 2000). In supplemental Discussion 1, available at www.jneurosci.org as supplemental material, we combine the results from a previous human attention study using ECoG (Ray et al., 2008a) and the present monkey LFP study to determine the increase in firing rate required to explain the increase in ECoG high-gamma because of attention. We show that the increase in firing rate must be unreasonably high (much larger than the increase observed in comparable neurophysiological studies of attention) to explain the results. This comparison supports the idea that attention enhances the synchronization between neurons, and that ECoG high-gamma power is an index of this synchrony.

Discussion

We studied the relationship between high-gamma activity and neuronal firing at the level of local field potentials which reflect the activity of a small population of neurons near a microelectrode, and developed a simple model to explore the relative contributions of an increase in firing rate versus synchrony on ECoG
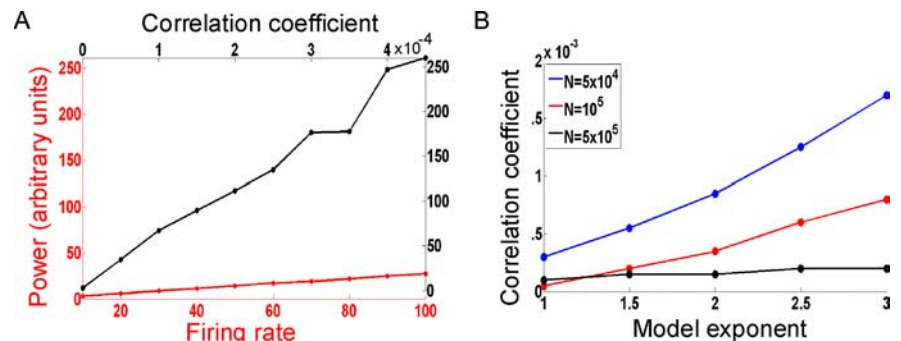

Figure 5. Comparison of power for random firing versus correlated firing. *A*, High-gamma power of a randomly firing population of 10^5 neurons with model exponent (*n* in Eq. 2) set to 2 (red trace) as the firing rate increases from 10 to 100 spikes/s, superimposed with the high-gamma power of the same population of neurons firing with a correlation coefficient that increases from 0 to 0.00045 (with firing rate fixed at 10 spikes/s). *B*, Correlation coefficient required to match the high-gamma power of a randomly firing population with a firing rate of 100 spikes/s, for different values of *N* (size of the neural population) and model exponent.

data, which records the activity of a large population ($>10^5$) of neurons. There are two main findings. First, we show that LFP high-gamma power is tightly correlated with the instantaneous firing rate of the neural population near the recording electrode. Second, using a model to estimate the ECoG signals arising from different population firing parameters, we show that both an increase in firing rate and synchrony lead to an increase in ECoG high-gamma power. However, increases in ECoG high-gamma

activity because of a large increase (10-fold) in population firing rate can be matched by a small increase ($\sim$1%) in neuronal firing synchrony. Thus, while at the level of LFP, high-gamma activity may only reflect the firing rate of the neural population near the microelectrode, at a larger level of integration such as ECoG, it is possibly an index of neural synchrony in the underlying cortical population.

Significance of high-gamma oscillations

Our results are consistent with a growing number of LFP studies suggesting a link between high-gamma oscillations and spiking activity (Liu and Newsome, 2006; Belitski et al., 2008). The observed correlation between high-gamma power and population spiking activity in our study is much stronger than in earlier work. One reason could be due to the use of matching pursuit for generating the time-frequency spectrum, because the Gabor function dictionaries used in MP provide the best time-frequency resolution possible in agreement with the uncertainty principle, and consequently provide an excellent description of the time-frequency properties of nonstationary signals. In supplemental Discussion 3, available at www.jneurosci.org as supplemental material, we compare the performance of MP versus traditional methods such as Fourier Transform for the representation of highly nonstationary LFP signals. The multiscale decomposition of MP allows sharp transients in the LFP signal (likely because of spiking activity) to be represented by functions that have a narrow temporal support, rather than oscillatory functions with a temporal support of hundreds of milliseconds (typical in methods such as Short Time Fourier Transform/Multi-tapering). Further details can be found in Ray et al., 2008b.

Other than these LFP studies, high-gamma power augmentation has been observed consistently in a large number of ECoG studies in a variety of functional domains, including motor (Crone et al., 1998; Ohara et al., 2000; Pfurtscheller et al., 2003; Brovelli et al., 2005; Miller et al., 2007), visual (Lachaux et al., 2005; Tallon-Baudry et al., 2005), auditory (Crone et al., 2001a; Edwards et al., 2005; Trautner et al., 2006), somatosensory (Ray et al., 2008a), and language cortices (Crone et al., 2001b; Mainy et al., 2007b; Jung et al., 2008). In addition, high-gamma activity is modulated during selective attention (Tallon-Baudry et al., 2005; Jung et al., 2008; Ray et al., 2008a), working memory (Canolty et al., 2006; Mainy et al., 2007a), and recognition memory (Sederberg et al., 2007). Furthermore, a number of noninvasive studies using either scalp EEG (Ball et al., 2008) or magnetoencephalography (Kaiser and Lutzenberger, 2005; Gross et al., 2007; Hauck et al., 2007; Dalal et al., 2008) have reported gamma responses that include, or are restricted to, high-gamma frequencies. The seeming ubiquity of high-gamma responses during cortical activation, as well as their high degree of specificity for the expected location, timing, and stimulus-selectivity of cortical activation, suggests that high-gamma activity constitutes a universal index of cortical processing. This is not surprising given its close relationship to neuronal spiking.

Our results suggest a crucial role for high-gamma activity in linking the signals observed in microelectrode studies with signals obtained from macroelectrode studies, such as intracranial EEG studies in humans. LFPs are thought to represent the synaptic activity of a few thousand neurons, depending on the tip diameter used for the recording (Nunez, 1981, 1995). Whereas lower frequency activity in the LFP may be due to the activity of a larger population, higher frequencies typically reflect a smaller population (Nunez, 1981). Indeed, frequencies greater than $\sim$300 Hz are probably dominated by the currents associated with

action potentials (Logothetis, 2002). In this respect, it is not surprising that high-frequency activity is tightly coupled to the firing of a few neurons. More surprising is the range of frequencies that are correlated with spiking activity; we show that power in a frequency range as low as 60–200 Hz is tightly coupled to the firing rates of a small population of neurons. The higher frequency components of LFPs have a greater relative contribution from action potentials, whereas the size of the neural population (that generates the activity at that frequency) decreases with increasing frequency (Nunez, 1981). The high-gamma frequency range (60–200 Hz) appears to be well suited for studying the spiking activity of a relatively small population of neurons in LFP recordings.

Furthermore, our modeling analysis shows that an increase in cross-correlation of as low as 10^{-4} over a large population of neurons may lead to a large increase in high-gamma power. An increase of this magnitude would be very difficult to detect using single unit measures with analysis methods such as pairwise cross-correlation. This may explain why, although there are several studies showing an increase in synchronization at the level of multi units or LFP with selective attention (Fries et al., 2001; Bichot et al., 2005; Womelsdorf et al., 2006), fewer studies have reported an increase in synchrony at the level of single units (Steinmetz et al., 2000). The cross-correlation values reported by Steinmetz et al. (2000) were very small but were shown to be significant. High-gamma activity may be a more reliable and robust reflection of synchronization than pairwise cross-correlation, especially when recorded at a high level of neural integration like subdural ECoG. However, whereas our modeling study shows the relative effects of increases in firing rate and spike synchrony in large populations of neurons, these are 'idealized' results aimed to reinforce the theoretical results developed in the appendix. These modeling results are obtained under a series of assumptions and must be complemented by neurophysiological studies before the relative roles of rates and synchrony can be unequivocally determined. In supplemental Discussion 2, available at www.jneurosci.org as supplemental material, we address some of the limitations of the model in further detail, and discuss possible experiments that can address some of the concerns.

Low-gamma versus high-gamma activity

Several functional mechanisms have been suggested for low-gamma oscillations, such as an increase in single unit synchronization (Singer and Gray, 1995; Engel et al., 2001; Salinas and Sejnowski, 2001; Buzsáki and Draguhn, 2004; Womelsdorf et al., 2007), controlling the communication channels between input and output neural assemblies (Fries, 2005; Womelsdorf and Fries, 2006), and setting a temporal reference frame so that latency or rank-ordering of spike times with respect to the gamma cycle can carry information (Buzsáki and Chrobak, 1995; Buzsáki and Draguhn, 2004; Fries et al., 2007). Furthermore, these gamma oscillations have been observed during several higher cortical processes such as selective attention (Tiitinen et al., 1993; Fries et al., 2001; Womelsdorf et al., 2006), sensorimotor integration (Murthy and Fetz, 1992; Roelfsema et al., 1997), binding of distributed representations (Gray et al., 1989; Singer and Gray, 1995), working memory (Pesaran et al., 2002), associative learning (Miltner et al., 1999), and conscious perception (Singer and Gray, 1995; Rodriguez et al., 1999; Meador et al., 2002).

The results presented in this study are not inconsistent with any of these suggested roles of gamma oscillations. However, our results point to an alternative hypothesis regarding the physiological origin of low-gamma oscillations. Just as an increase in

high-gamma could be attributable to an increase in spike synchronization within the neural population, an increase in low-gamma power could be attributable to an increase in synchronization in synaptic inputs, because synaptic activity is correlated with the low-gamma frequency range (Niessing et al., 2005; Viswanathan and Freeman, 2007). This is consistent with our finding that low-gamma power increases before the increase in firing rate (Fig. 1B, middle panel). Thus, while high-gamma power could be a neural correlate of synchronized output of the cortex, low-gamma power could be a correlate of synchronized input to the cortex. Although these hypotheses suggest no "functional" role of low- and high-gamma oscillations, these oscillations could nevertheless reflect ongoing neural processes related to dynamic cortical functions.

Regardless of whether high-gamma oscillations play any role in cortical processing, our results suggest that high-gamma activity in electrophysiological recordings of a large population (like ECoG) could be a useful indicator of the firing dynamics of the neural population whose activity is being recorded. This key finding could potentially be used to characterize the nature of neural processing used in different cognitive tasks, in particular, whether the information is carried entirely by the mean rate of action potentials (a rate code) or whether the precise occurrence times of action potentials also carries information (a temporal code). For example, in supplemental Discussion 1, available at www.jneurosci.org as supplemental material, we argue that an increase in ECoG high-gamma power attributable to attention is better explained by increases in neural synchrony than by firing rate. Similar studies using ECoG and other invasive techniques, e.g., microelectrode recordings, are expected to enhance our understanding of the role of gamma oscillations during different cognitive tasks and the nature of cortical processing associated with these oscillations.

Appendix 1

In this appendix, we try to estimate the high-gamma power in ECoG using simple mathematical arguments. Although both an increase in firing rate and an increase in synchrony in the neural population may lead to an increase in high-gamma activity in ECoG, previous theoretical studies have suggested that for a large population of neurons (like the one recorded by the ECoG electrode), the ratio of activity recorded from a coherent subpopulation of size M versus that from an incoherent subpopulation of size N, is $M/\sqrt{N}$ (Nunez, 1981, 1995). For instance, for a population of 10^5 neurons (the typical size of a macrocolumn; the ECoG data generally represent a much larger population), even if only 1% of the population is synchronized, the activity of this synchronized subpopulation will be $10^3/\sqrt{10^5}$ (approximately three times more) than that of the incoherent subpopulation.

A crude measure of the ECoG high-gamma activity is the local fluctuation (SD) in population firing rate, which prevents high-gamma oscillations from canceling each other out. ECoG high-gamma power (proportional to the square of the activity) will thus be proportional to the variance in the firing rate. We compute the variance in firing rate under the following three conditions described in the study: (1) The entire population fires asynchronously; (2) A fraction (θ) of the population fires in perfect synchrony, whereas the remaining population fires asynchronously; (3) the firing rates in the population are correlated such that any two spike trains have a correlation coefficient of χ.

Let the size of the population be N, with a firing probability of p in a bin of size Δt. Let X be the number of spikes in this bin. We estimate the variance $\text{Var}(X)$ under the three conditions mentioned above. Let $q = 1-p$.

Case 1: Asynchronous firing. $X \sim \text{Binomial}(N,p)$; $\text{Var}(X) = Npq$.

Thus, the power increases linearly with N.

Case 2: A fraction θ of neurons fire synchronously.

Let X_1 be the total number of spikes from the synchronous population (of size $N\theta$). $X_1 \sim (N\theta)\text{Binomial}(1,p)$ (i.e., either $N\theta$ or 0 with probability p and q, respectively).

Let X_2 be the total number of spikes from the asynchronous population (of size $N(1-\theta)$). $X_2 \sim \text{Binomial}(N(1-\theta),p)$; $X = X_1 + X_2$; $\text{Var}(X) = \text{Var}(X1) + \text{Var}(X2)$ (the two random variables are independent); $= (N^2\theta^2)pq + N(1-\theta)pq$. For large values of N, the second term is negligible. The power increases as N^2, consistent with the earlier theoretical arguments.

Case 3: Any two spike trains have a correlation coefficient of χ. Such a population of neurons can be constructed by first randomly generating $N + 1$ spike trains, setting the $N + 1^{\text{th}}$ as a reference spike train, and then switching, with probability $\sqrt{\chi}$, the state of a time bin in each of these spike trains to the reference spike train (Mikula and Niebur, 2003; Niebur, 2007).

Let $c = \sqrt{\chi}$ and $q = 1-p$. Suppose N_1 states get switched. Then $N_1 \sim \text{Binomial}(N,c)$. Suppose the state of this bin in the reference spike train is Z. Then $Z \sim \text{Binomial}(1,p)$. Let Y be the number of spikes obtained from the remaining $N–N_1$ spike trains (whose state has not been switched). Then $Y \sim \text{Binomial}(N–N_1,p)$. $X = N_1.Z + Y$; $\text{Var}(X) = E(\text{var}(X/N_1)) + \text{var}(E(X/N_1))$ (law of total variance).

First term:

$$E(\text{var}(X/N_1)) = \sum_{k=0}^{N} P(N_1 = k)\text{var}(X/N_1 = k).$$

But $\text{var}(X/N_1 = \text{k}) = \text{var}(kZ) + \text{var}(Y)$,
where $Y \sim B(N–k,p)$; $= k^2pq + (N–k)pq$.

Hence,

$$E(\text{var}(X/N_1)) = pq \sum_{k=0}^{N} P(N = k)(k^2 + N - k)$$

$$= pq[E(N_1{}^2) + N - E(N_1)]$$

$$= pq[\text{var}(N_1) + (E(N_1))^2 + N - E(N_1)]$$

$$= pq[Nc(1 - c) + (Nc)^2 + N - Nc]$$

$$= pq[N^2c^2 + N(1 - c^2)]$$

$$= pq[N^2\chi + N(1 - \chi)].$$

Second term: $\text{var}(E(X/N_1))$.

However,

$$E(X/N_1) = \sum_{k=0}^{N} P(N_1 = k)\, E(X/N_1 = k) = \sum_{k=0}^{N} P(N_1 = k)(kp$$

$$+ (N - k)p) = Np,$$

so that $\text{var}(E(X/N_1)) = 0$;

thus, $\text{Var}(X) = pq(N^2\chi + N(1-\chi))$.

These simple mathematical derivations are consistent with the

results shown in Figures 4*C* and 5*A*. The power increases linearly with the firing rate (p) for the asynchronous case in Figure 4*C* (red line), increases as θ^2 for the synchronous case (black line), and increases linearly with χ in Figure 5*A* (black line).

References

Ball T, Demandt E, Mutschler I, Neitzel E, Mehring C, Vogt K, Aertsen A, Schulze-Bonhage A (2008) Movement related activity in the high gamma range of the human EEG. Neuroimage 41:302–310.

Belitski A, Gretton A, Magri C, Murayama Y, Montemurro MA, Logothetis NK, Panzeri S (2008) Low-frequency local field potentials and spikes in primary visual cortex convey independent visual information. J Neurosci 28:5696–5709.

Bichot NP, Rossi AF, Desimone R (2005) Parallel and serial neural mechanisms for visual search in macaque area V4. Science 308:529–534.

Brovelli A, Lachaux JP, Kahane P, Boussaoud D (2005) High gamma frequency oscillatory activity dissociates attention from intention in the human premotor cortex. Neuroimage 28:154–164.

Buzsáki G, Chrobak JJ (1995) Temporal structure in spatially organized neuronal ensembles: a role for interneuronal networks. Curr Opin Neurobiol 5:504–510.

Buzsáki G, Draguhn A (2004) Neuronal oscillations in cortical networks. Science 304:1926–1929.

Canolty RT, Edwards E, Dalal SS, Soltani M, Nagarajan SS, Kirsch HE, Berger MS, Barbaro NM, Knight RT (2006) High gamma power is phase-locked to theta oscillations in human neocortex. Science 313:1626–1628.

Crone NE, Miglioretti DL, Gordon B, Lesser RP (1998) Functional mapping of human sensorimotor cortex with electrocorticographic spectral analysis. II. Event-related synchronization in the gamma band. Brain 121:2301–2315.

Crone NE, Boatman D, Gordon B, Hao L (2001a) Induced electrocorticographic gamma activity during auditory perception. Brazier Award-winning article, 2001. Clinical Neurophysiology 112:565–582.

Crone NE, Hao L, Hart J Jr, Boatman D, Lesser RP, Irizarry R, Gordon B (2001b) Electrocorticographic gamma activity during word production in spoken and sign language. Neurology 57:2045–2053.

Crone NE, Sinai AS, Korzeniewska A (2006) High-frequency gamma oscillations and human brain mapping with electrocorticography. Prog Brain Res 159: 275–295.

Dalal SS, Guggisberg AG, Edwards E, Sekihara K, Findlay AM, Canolty RT, Berger MS, Knight RT, Barbaro NM, Kirsch HE, Nagarajan SS (2008) Five-dimensional neuroimaging: localization of the time-frequency dynamics of cortical activity. Neuroimage 40:1686–1700.

de la Rocha J, Doiron B, Shea-Brown E, Josić, K, Reyes A (2007) Correlation between neural spike trains increases with firing rate. Nature 448:802–806.

Edwards E, Soltani M, Deouell LY, Berger MS, Knight RT (2005) High gamma activity in response to deviant auditory stimuli recorded directly from human cortex. J Neurophysiol 94:4269–4280.

Engel AK, Fries P, Singer W (2001) Dynamic predictions: oscillations and synchrony in top-down processing. Nat Rev Neurosci 2:704–716.

Fries P (2005) A mechanism for cognitive dynamics: neuronal communication through neuronal coherence. Trends Cogn Sci 9:474–480.

Fries P, Reynolds JH, Rorie AE, Desimone R (2001) Modulation of oscillatory neuronal synchronization by selective visual attention. Science 291:1560–1563.

Fries P, Nikolić D, Singer W (2007) The gamma cycle. Trends in Neurosciences 30:309–316.

Gold C, Henze DA, Koch C, Buzsaki G (2006) On the origin of the extracellular action potential waveform: a modeling study. J Neurophysiol 95:3113–3128.

Gray CM, König P, Engel AK, Singer W (1989) Oscillatory responses in cat visual cortex exhibit inter-columnar synchronization which reflects global stimulus properties. Nature 338:334–337.

Gross J, Schnitzler A, Timmermann L, Ploner M (2007) Gamma oscillations in human primary somatosensory cortex reflect pain perception. Plos Biology 5:1168–1173.

Hauck M, Lorenz J, Engel AK (2007) Attention to painful stimulation enhances gamma-band activity and synchronization in human sensorimotor cortex. J Neurosci 27:9270–9277.

Jung J, Mainy N, Kahane P, Minotti L, Hoffmann D, Bertrand O, Lachaux JP (2008) The neural bases of attentive reading. Hum Brain Mapp 29:1193–1206.

Kaiser J, Lutzenberger W (2005) Human gamma-band activity: a window to cognitive processing. Neuroreport 16:207–211.

Lachaux JP, George N, Tallon-Baudry C, Martinerie J, Hugueville L, Minotti L, Kahane P, Renault B (2005) The many faces of the gamma band response to complex visual stimuli. Neuroimage 25:491–501.

Liu J, Newsome WT (2006) Local field potential in cortical area MT: stimulus tuning and behavioral correlations. J Neurosci 26:7779–7790.

Logothetis NK (2002) The neural basis of the blood-oxygen-level-dependent functional magnetic resonance imaging signal. Philos Trans R Soc Lond B Biol Sci 357:1003–1037.

Logothetis NK, Kayser C, Oeltermann A (2007) In vivo measurement of cortical impedance spectrum in monkeys: implications for signal propagation. Neuron 55:809–823.

Mainy N, Kahane P, Minotti L, Hoffmann D, Bertrand O, Lachaux JP (2007a) Neural correlates of consolidation in working memory. Human Brain Mapping 28:183–193.

Mainy N, Jung J, Baciu M, Kahane P, Schoendorff B, Minotti L, Hoffmann D, Bertrand O, Lachaux JP (2007b) Cortical dynamics of word recognition. Hum Brain Mapp, in press.

Mallat S, Zhang Z (1993) Matching pursuit with time-frequency dictionaries. IEEE Trans Signal Proc 41:3397–3415.

Malmivuo J, Plonsey R (1995) Bioelectromagnetism. New York: Oxford UP.

Meador KJ, Ray PG, Echauz JR, Loring DW, Vachtsevanos GJ (2002) Gamma coherence and conscious perception. Neurology 59:847–854.

Mikula S, Niebur E (2003) The effects of input rate and synchrony on a coincidence detector: analytical solution. Neural Comput 15:539–547.

Miller KJ, Leuthardt EC, Schalk G, Rao RP, Anderson NR, Moran DW, Miller JW, Ojemann JG (2007) Spectral changes in cortical surface potentials during motor movement. J Neurosci 27:2424–2432.

Miltner WH, Braun C, Arnold M, Witte H, Taub E (1999) Coherence of gamma-band EEG activity as a basis for associative learning. Nature 397:434–436.

Mountcastle VB, Reitboeck HJ, Poggio GF, Steinmetz MA (1991) Adaptation of the Reitboeck method of multiple microelectrode recording to the neocortex of the waking monkey. J Neurosci Methods 36:77–84.

Murthy VN, Fetz EE (1992) Coherent 25- to 35-Hz oscillations in the sensorimotor cortex of awake behaving monkeys. Proc Natl Acad Sci U S A 89:5670–5674.

Niebur E (2007) Generation of synthetic spike trains with defined pairwise correlations. Neural Comput 19:1720–1738.

Niessing J, Ebisch B, Schmidt KE, Niessing M, Singer W, Galuske RA (2005) Hemodynamic signals correlate tightly with synchronized gamma oscillations. Science 309:948–951.

Noctor SC, Palmer SL, McLaughlin DF, Juliano SL (2001) Disruption of layers 3 and 4 during development results in altered thalamocortical projections in ferret somatosensory cortex. J Neurosci 21:3184–3195.

Nunez PL (1981) Electrical fields of the brain: the neurophysics of EEG. New York: Oxford UP.

Nunez PL (1995) Neocortical dynamics and human EEG rhythms. Oxford: Oxford UP.

Ohara S, Ikeda A, Kunieda T, Yazawa S, Baba K, Nagamine T, Taki W, Hashimoto N, Mihara T, Shibasaki H (2000) Movement-related change of electrocorticographic activity in human supplementary motor area proper. Brain 123:1203–1215.

Pesaran B, Pezaris JS, Sahani M, Mitra PP, Andersen RA (2002) Temporal structure in neuronal activity during working memory in macaque parietal cortex. Nat Neurosci 5:805–811.

Pfurtscheller G, Graimann B, Huggins JE, Levine SP, Schuh LA (2003) Spatiotemporal patterns of beta desynchronization and gamma synchronization in corticographic data during self-paced movement. Clin Neurophysiol 114:1226–1236.

Ray S, Niebur E, Hsiao SS, Sinai A, Crone NE (2008a) High-frequency gamma activity (80–150 Hz) is increased in human cortex during selective attention. Clin Neurophysiol 119:116–133.

Ray S, Hsiao SS, Crone NE, Franaszczuk PJ, Niebur E (2008b) Effect of stimulus intensity on the spike-local field potential relationship in the secondary somatosensory cortex. J Neurosci 28:7334–7343.

Rodriguez E, George N, Lachaux JP, Martinerie J, Renault B, Varela FJ (1999)

Perception's shadow: long-distance synchronization of human brain activity. Nature 397:430–433.

Roelfsema PE, Engel AE, König P, Singer W (1997) Visuomotor integration is associated with zero time-lag synchronization among cortical areas. Nature 385:157–161.

Salinas E, Sejnowski TJ (2001) Correlated neuronal activity and the flow of neural information. Nat Rev Neurosci 2:539–550.

Scherberger H, Jarvis MR, Andersen RA (2005) Cortical local field potential encodes movement intentions in the posterior parietal cortex. Neuron 46:347–354.

Schoffelen JM, Oostenveld R, Fries P (2005) Neuronal coherence as a mechanism of effective corticospinal interaction. Science 308:111–113.

Sederberg PB, Schulze-Bonhage A, Madsen JR, Bromfield EB, Litt B, Brandt A, Kahana MJ (2007) Gamma oscillations distinguish true from false memories. Psychol Sci 18:927–932.

Singer W, Gray CM (1995) Visual feature integration and the temporal correlation hypothesis. Ann Rev Neurosci 18:555–586.

Steinmetz PN, Roy A, Fitzgerald PJ, Hsiao SS, Johnson KO, Niebur E (2000) Attention modulates synchronized neuronal firing in primate somatosensory cortex. Nature 404:187–190.

Tallon-Baudry C, Bertrand O, Hénaff MA, Isnard J, Fischer C (2005) Attention modulates gamma-band oscillations differently in the human lateral occipital cortex and fusiform gyrus. Cereb Cortex 15:654–662.

Tiitinen H, Sinkkonen J, Reinikainen K, Alho K, Lavikainen J, Näätänen R (1993) Selective attention enhances the auditory 40-Hz transient response in humans. Nature 364:59–60.

Trautner P, Rosburg T, Dietl T, Fell J, Korzyukov OA, Kurthen M, Schaller C, Elger CE, Boutros NN (2006) Sensory gating of auditory evoked and induced gamma band activity in intracranial recordings. Neuroimage 32:790–798.

Viswanathan A, Freeman RD (2007) Neurometabolic coupling in cerebral cortex reflects synaptic more than spiking activity. Nat Neurosci 10:1308–1312.

Womelsdorf T, Fries P (2006) Neuronal coherence during selective attentional processing and sensory-motor integration. J Physiol Paris 100:182–193.

Womelsdorf T, Fries P, Mitra PP, Desimone R (2006) Gamma-band synchronization in visual cortex predicts speed of change detection. Nature 439:733–736.

Womelsdorf T, Schoffelen JM, Oostenveld R, Singer W, Desimone R, Engel AK, Fries P (2007) Modulation of neuronal interactions through neuronal synchronization. Science 316:1609–1612.